

Trabalho de conclusão de curso

Exploring the strong-correlation puzzle in FeO via DFT+U

Daniel de Martini Rivera Ferreira^{1,*} and Lucas Almeida Miranda Barreto^{1,†}

¹*Center of Natural and Human Sciences (CCNH),
Federal University of ABC, Santo Andre-SP, Brazil*

The strong Coulomb electron correlation plays a key role in the band gap description of Mott insulators. Therefore, more than the traditional band theory is needed to model those materials. Density Functional Theory (DFT), for example, predicts inaccurate properties for Mott insulators. Among the different strategies to address this limitation, an extension of DFT based on the Hubbard Hamiltonian (DFT+U) provides a considerable improvement to depict systems with strong correlated electrons. In this work, the application of DFT+U aimed to obtain the main experimental results for bulk and (111) surface FeO. The choice of the surface is justified by the [111] orientation of the spins in the iron atoms. The proposed model predicted that the magnetic configuration of the bulk ground state is antiferromagnetic, in agreement with experimental data. Furthermore, the structural, electronic, and magnetic properties of the bulk were successfully reproduced. The model also predicted that the ground state of the (111) surface is antiferromagnetic, and the surface states were found to be metallic.

1. INTRODUCTION AND MOTIVATIONS

The development of quantum mechanics enabled its application in many different branches of physics, from describing interactions of fundamental particles, as seen in QED [1], to exotic materials properties, like topological matter [2, 3]. Indeed, quoting P. Dirac: *The underlying physical laws necessary for the mathematical theory of a large part of physics and the whole of chemistry are thus completely known, and the difficulty is only that the exact application of these laws leads to equations much too complicated to be soluble. It therefore becomes desirable that approximate practical methods of applying quantum mechanics should be developed, which can lead to an explanation of the main features of complex atomic systems without too much computation*

*Electronic address: daniel.ferreira@aluno.ufabc.edu.br

†Electronic address: lucas.barreto@ufabc.edu.br

[4].

In condensed matter physics, it is desirable to deal with N body problems in the thermodynamic limit ($N \rightarrow \infty$), but the equations often become too complicated to deal with [5]. Considering symmetries and simplifications to the theory is a good path to calculate materials properties in a feasible way [6, 7]. Bloch theorem and the development of DFT [8, 9] are among the main methods used to deal with this kind of problem.

Nonetheless, just symmetry considerations plus simplifications fail to describe a specific class of materials, the *strongly correlated systems* [10]. This characterizes the strong-correlation puzzle. The behavior of this kind of quantum matter is not well understood in physics, as we can cite among them the false metals, Mott insulators and high temperature superconductors [10, 11]. Fundamental properties are qualitatively mispredicted, like the Mott insulators, which are experimentally insulators but predicted as metals by state-of-the-art electronic structure calculation techniques. This leads to the question: why is this kind of discrepancy appearing?

The most accepted hypothesis today is that strongly correlated effects are related to interactions between electrons inside the materials [10]. The effects of these interactions becomes clearer in the Hubbard model, which explores an extension to the tight binding model taking coulomb interaction between electrons into account [12]. Recent works show that merging Hubbard based methods with DFT can describe Transition Metal Oxides' (TMO's) electronic properties in good agreement with experiments [13].

Hence, in this project, we use DFT with a correction based on the Hubbard Hamiltonian to model a prototypical TMO: ferrous oxide (FeO). This material is an antiferromagnetic (AFM) [14] TMO and Mott insulator with Rock Salt crystal structure. Electronic, magnetic and structural properties were calculated both in the bulk and the (111) surface of this material. FeO was the chosen system since it is simple enough to get the main physical intuitions about strongly correlated systems.

2. THEORETICAL FOUNDATIONS

2.1. Condensed matter physics and the N -body problem

Quantum mechanics, developed in the 20th century [5], is a theory that breaks paradigms, and its postulates are based on observations [15]. Max Planck, one of the fathers of quantum mechanics, has a constant (h) named after him, which gives the theory its characteristic of being a

generalization of classical mechanics that is useful for very small scales. Determining the properties of materials described by quantum theory is a highly complicated process but in extreme agreement with reality.

The problem boils down to solving the basic equation of quantum mechanics, the Schrödinger equation, given as follows [16]:

$$\hat{H} |\Psi(t)\rangle = i\hbar \frac{d}{dt} |\Psi(t)\rangle, \quad (1)$$

where \hat{H} denotes the Hamiltonian operator of the system, \hbar is the reduced Planck constant, i is the imaginary unit, and $|\psi(t)\rangle$ is a vector that represents the state of the system defined in the Hilbert space \mathcal{H} , the abstract vector space of state vectors of a quantum system. To extract the physics we evaluate the projected state, for example, in configuration space, known as the wave function, through the time-independent Schrödinger equation obtained by the method of separation of variables.

$$\begin{aligned} \langle \mathbf{r} | \Psi(t) \rangle &= \Psi(\mathbf{r}, t) = \psi(\mathbf{r})T(t) \Rightarrow \\ &\Rightarrow \hat{H}\psi(\mathbf{r}) = E\psi(\mathbf{r}). \end{aligned} \quad (2)$$

This work focuses primarily on the study of electronic structures in a set of atoms. Atoms are primarily composed of a positively charged nucleus (protons and neutrons) and negatively charged electrons. Thus, the relevant interaction is the electromagnetic interaction. Therefore, the Hamiltonian of the system already with the Born-Oppenheimer approximation [17], taking into account all the interactions we are aware of, in a pure description of quantum mechanics, is [5]:

$$\hat{H} = \left[-\frac{\hbar^2}{2m} \sum_{i=1}^N \nabla_i^2 + \sum_{i=1}^N V(\mathbf{r}_i) + \frac{1}{2} \sum_{i=1}^N \sum_{i \neq j}^N U(\mathbf{r}_i, \mathbf{r}_j) \right], \quad (3)$$

with m being the mass of the electron. The first term of the Hamiltonian describes the total kinetic energy of the system, the second term represents the Coulomb interaction of the electrons with the nuclei, and the third term indicates the electron-electron Coulomb interaction, with the constant 1/2 inserted to avoid double counting of particles [18].

The major problem is that, as one can see in equation 2, the solution is $\psi(\mathbf{r}_i)$, with i ranging up to the number N of electrons in the system, meaning it is dependent on $3N$ dimensions. It is evident that the problem becomes infeasible when dealing with situations studied in condensed matter, which involve numerous atoms and, consequently, electrons. Thus, solving the problem through the traditional description of quantum mechanics becomes unrealistic [5].

New ideas and approaches are necessary to describe electronic properties of condensed matter systems. Taking crystal symmetries into account gives a great insight on the electronic wavefunction form, besides describing well the energy eigenvalues of the system.

2.2. Electronic structure calculations: from symmetries to DFT

Symmetries in crystals is a well studied area in physics [6, 19]. These investigations gave birth to important areas in group theory, such as the *point groups* and *space groups*, which are the point groups with the addition of translations [19]. An important theorem in condensed matter comes from translational symmetry in crystals, named the Bloch's theorem. There are many ways to derive it, and the most didactic way, in the author's view, is done in the appendix A. Consider a crystal with translational symmetry described by a periodic potential $\hat{V} = V(\hat{\mathbf{r}} + \mathbf{a}) = V(\hat{\mathbf{r}})$, like shown in figure 1, the wavefunction inside this crystal will take the form below:

$$\psi_{n\mathbf{k}}(\mathbf{r}) = u_{n\mathbf{k}}(\mathbf{r})e^{i\mathbf{k}\cdot\mathbf{r}}, \quad (4)$$

with $u_{n\mathbf{k}}(\mathbf{r}) = u_{n\mathbf{k}}(\mathbf{r} + \mathbf{a})$ respecting the same translational periodicity of the potential. Here k represents the state wave vector. To understand electronic properties in materials, one could imagine the following toy model. Considering a one dimensional periodic potential \hat{V} , illustrated by figure 1, one can wonder what are the accessible states for electron's occupation. This question can be answered if we solve the Schrödinger equation with the periodic potential \hat{V} , given below:

$$\left[-\frac{\hbar^2}{2m}\nabla^2 + \hat{V} \right] \psi(\mathbf{r}) = E \psi(\mathbf{r}). \quad (5)$$



FIG. 1: Translational symmetry in a 1D crystal.

If one substitutes equation A2 into the Schrödinger equation of our model, the result is [7]:

$$\left[\frac{1}{2m} (-i\hbar\nabla + \hbar\mathbf{k})^2 + \hat{V} \right] u_{n\mathbf{k}}(\mathbf{r}) = E_{n\mathbf{k}} u_{n\mathbf{k}}(\mathbf{r}), \quad (6)$$

where the subscript n refers to the energy eigenstate. The main steps of this derivation are

explicitly shown in appendix B. It can be observed that, since $u_{n\mathbf{k}}$ is different for each wave vector \mathbf{k} , the energy $E_{n\mathbf{k}} \equiv E_n(\mathbf{k})$ also becomes dependent on \mathbf{k} in the \mathbf{k} continuous limit. Therefore, for each different \hat{V} , we have a continuous function $E_n(\mathbf{k})$, known as dispersion relation. This unique mapping characterizes different bands for different materials. The dispersion relations are known as bands, and this is referred to as band theory. Thus, if $n \in \{1, 2, 3, \dots, 20\}$, there are 20 bands that are solutions of equation 6. Hence, the band structure is obtained, as depicted in figure 2.

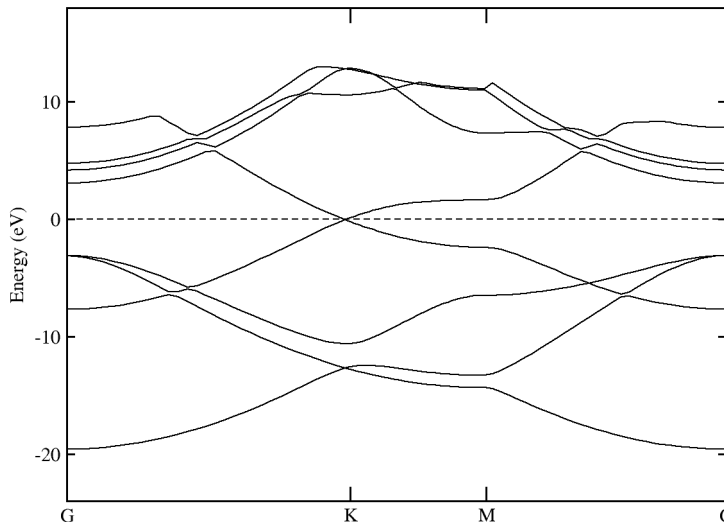


FIG. 2: Graphene band structure as an example. The x axis represent some high symmetry points in the 1st Brillouin zone on the k -space.

Band theory is a great way of calculating a material's electronic structure, thus inferring electronic properties of the system. Another great tool to realize electronic properties of materials is the Density Of States (DOS), given by equation 7. This is one of the many k -space integrals which are done in this work.

$$\eta(E) = \sum_n \int \frac{d^3k}{\Omega_{BZ}} \delta(E - E_{n\mathbf{k}}). \quad (7)$$

Here, Ω_{BZ} is the 1st Brillouin zone volume and $\delta(E - E_{n\mathbf{k}})$ is the Dirac delta function. The relation between the DOS and the band structure becomes explicit, where there is a *capture* of the n allowed energy states $E_{n\mathbf{k}}$ from the Dirac delta function, integrated over the first Brillouin zone [7, 8]. These captured n states are summed, resulting in the density of states as a function of energy. In other words, the DOS represents the number of allowed states per unit of energy.

However, one should notice that interactions between electrons are completely ignored [8], since the fermionic particles just occupy the eigenstates obtained from equation 6, following the Pauli

exclusion principle [20]. In this way, density functional theory is a great and much used solution to calculate electronic properties of real materials.

2.3. Density functional theory: electronic and magnetic properties

Density Functional Theory (DFT) is one of the most popular approaches to solve the many-body problem, and it holds significant importance in condensed matter. Its recognition and applicability granted the Nobel Prize in Chemistry for its developers in 1998 [9]. Its applications go from calculating binding energy of molecules to electronic and magnetic properties of complex solids [21]. Maybe its large range of applicability is due to its simplicity in comparison with other standard quantum approaches to condensed matter problems [5, 7, 21].

The main idea of DFT is to promote the charge density $\rho(\mathbf{r})$ from one of the many observables to the main object of the system [21]. This is done by using the *ansatz* $\rho(\mathbf{r}) = 2e \sum_i |\psi_i(\mathbf{r})|^2$, where the parameter e represents the charge of the electron, and $\psi_i(\mathbf{r})$ are the Kohn-Sham orbitals, or the solutions of the main equations in DFT - the Kohn-Sham (KS) equations. This step transforms a problem of i interacting bodies into i single-body problems [7, 21], a statement that will become clearer as the discussion progresses.

Hohenberg and Kohn theorems are what define DFT. Both of them are crucial to construct the KS equations and are explicitly shown below:

- i*) In the ground state, the electronic density $\rho(\mathbf{r})$ uniquely determines the external potential, the Hamiltonian, and the energy of the system through a functional relation [5].
- ii*) The density $\rho(\mathbf{r})$ that minimizes the energy of the system is the ground state solution of the KS equations [5].

Thus, to construct the KS equations from scratch, one has to build the energy density functional, shown below, hence the name density functional theory. This functional can be built from physical arguments, and it won't be shown with details in this text. If one wants to read a more detailed construction, it is available in reference [7].

$$\begin{aligned}
 E[\rho(\mathbf{r})] = & -\frac{\hbar^2}{2m} \sum_i \int d^3r \psi_i^*(\mathbf{r}) \nabla^2 \psi_i(\mathbf{r}) + \int d^3r V(\mathbf{r}) \rho(\mathbf{r}) + \\
 & + \frac{e^2}{2} \int \int d^3r d^3r' \frac{\rho(\mathbf{r}) \rho(\mathbf{r}')}{|\mathbf{r} - \mathbf{r}'|} + E_{nuclei} + E_{XC}.
 \end{aligned} \tag{8}$$

Each term represent one form of energy: the total kinetic energy of the electrons, the total coulomb interaction between electrons and nuclei, the *mean field term* representing the electron-electron coulomb interaction (Hartree) [7] and the coulomb interaction between the nuclei [5]. The last term, E_{XC} , basically holds the unknown lost information about exchange and correlation energies mentioned before [5, 7]. This term is the heart of this project, and will be discussed soon.

The second theorem can be mathematically stated as [7]:

$$\frac{\delta}{\delta\rho}E[\rho(\mathbf{r})] = 0,$$

which is a functional derivative [21]. By applying the second theorem on equation 8, and using Lagrange multipliers, as done in reference [7], one can derive the KS equations:

$$\left[-\frac{\hbar^2}{2m}\nabla^2 + V_{eff}(\mathbf{r}) \right] \phi_i(\mathbf{r}) = \epsilon_i\phi_i(\mathbf{r}), \quad (9)$$

$$V_{eff}(\mathbf{r}) = V_{ext}(\mathbf{r}) + V_H(\mathbf{r}) + V_{XC}(\mathbf{r}).$$

Here, ϕ_i are the KS orbitals, the index i indicates the i^{th} single particle KS orbital, and ϵ_{nk} are the KS eigenvalues, $V_{ext}(\mathbf{r})$ represents the electron-nuclei interaction potential, $V_H(\mathbf{r})$ is the Hartree potential, which describes an effective classical *mean field* potential for electron-electron interaction, and $V_{XC}(\mathbf{r})$ is the exchange and correlation potential. This last term is related to the exchange and correlation functional by:

$$V_{XC} = \frac{\delta}{\delta\rho}E_{XC}[\rho(\mathbf{r})].$$

V_H and V_{XC} depend on $\rho(\mathbf{r})$, which makes DFT an exact theory if the analytic form of both V_H and V_{XC} are known. As the solutions of KS equations are the KS orbitals ϕ_i , which are the building blocks of ρ , one should solve this problem iteratively, following the steps shown below:

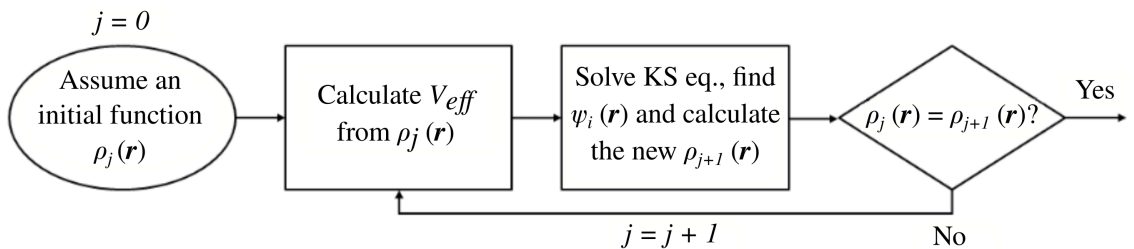


FIG. 3: Algorithm used to solve KS equations. Here j is the iteration number, or step. One can notice that a convergence criteria must be matched in order to end the iteration loop.

Putting Bloch's theorem into the KS orbitals yields to a similar result to that of equation 6:

$$\left[\frac{1}{2m} (-i\hbar\nabla + \hbar\mathbf{k})^2 + V_{eff}(\mathbf{r}) \right] u_{n\mathbf{k}}(\mathbf{r}) = \epsilon_{n\mathbf{k}} u_{n\mathbf{k}}(\mathbf{r}). \quad (10)$$

And that is the KS equations solved in figure's 3 algorithm. Unfortunately, the scientific community does not know the exact form of the term E_{XC} [5, 7], and results depend on approximation of the exchange and correlation effects, like the LDA [7] or PBE [22] (GGA) approximations [7]. This works well for some kinds of systems, which can be approximated as a Fermi gas [7]. In other words, essentially metals. But, as one will see in the next session, there are some materials that cannot be described with these kinds of approximations alone [10].

In the last section, one was presented to equation 6, where $E_{n\mathbf{k}}$ represented a band, or an energy eigenvalue corresponding to a state vector of the material ψ . Due to the differences in KS equations when compared to the Schrödinger equation, its eigenvectors ϕ_i and eigenvalues $\epsilon_{n\mathbf{k}}$ do not have this straightforward meaning anymore. Nevertheless, the KS eigenvalues are great approximate energy values, and they are useful to build band diagrams, as one can see in reference [7].

To end this session, magnetism in matter under the eyes of DFT is discussed. The characteristic magnetism of some materials has two sources: the magnetic moment arising from the orbital angular momentum of the electrons and the magnetic moment of the spins in the electrons that constitute the atoms of the system [8]. The orbital angular momentum gives rise to diamagnetic and paramagnetic materials, which will not be addressed in this work. Therefore, the discussions will be focused on materials whose magnetism arises as a consequence of the total spin of the electrons and exhibits ordering: ferromagnetic (FM) and antiferromagnetic (AFM) materials.

Spin is an internal degree of freedom present in all particles in the universe, a consequence of the relativistic nature described [15]. Paul Dirac was the first to demonstrate this fact, describing the electron's state as a four-dimensional spinor, a solution to his relativistic theory for the electron [15]. When treating the equation in the non-relativistic limit for an electron in a weak magnetic field, Dirac's spinor becomes the two-dimensional Pauli spinor $|\psi\rangle$, and the equation takes the form:

$$\left[\frac{1}{2m} \left(\hat{\mathbf{p}}^2 - (\hat{\mathbf{L}} + 2\hat{\mathbf{S}}) \cdot \mathbf{B} \right) + e\Phi \right] |\psi\rangle = E|\psi\rangle. \quad (11)$$

In equation 11, $\hat{\mathbf{p}}$ represents the conjugate momentum, $\hat{\mathbf{S}}$ the spin operator, \mathbf{B} the external magnetic field (which could be caused by the environment, in an FM material, for example [7]), $\hat{\mathbf{L}}$ is the orbital angular momentum and Φ is the electrostatic potential. By dealing with the case of

interest of this project, one can ignore $\hat{\mathbf{L}}$ and Φ , leading to the following equation:

$$\left[\frac{\hat{\mathbf{p}}^2}{2m} - \mu_B \hat{\boldsymbol{\sigma}} \cdot \mathbf{B} + \hat{V} \right] |\psi\rangle = E |\psi\rangle. \quad (12)$$

Where $\mu_B = \frac{e\hbar}{2m}$ is the Bohr magneton, a unit of measure that will be used later. In this equation, the first and last terms are multiplied by the identity matrix, which is omitted for the sake of simplicity. The symbol $\hat{\boldsymbol{\sigma}}$ represents the Pauli vector operator, where its components ($\hat{\sigma}_x, \hat{\sigma}_y, \hat{\sigma}_z$) are the Pauli matrices:

$$\hat{\sigma}_x = \begin{pmatrix} 0 & 1 \\ 1 & 0 \end{pmatrix}, \quad \hat{\sigma}_y = \begin{pmatrix} 0 & -i \\ i & 0 \end{pmatrix}, \quad \hat{\sigma}_z = \begin{pmatrix} 1 & 0 \\ 0 & -1 \end{pmatrix}. \quad (13)$$

In DFT, the KS equations take a similar form to equation 12, the difference lies in the potential $\hat{V} \rightarrow \hat{V}_{eff}$, the magnetic field $\mathbf{B} \rightarrow -\mathbf{B}_{xc}$ [7], and in the 2-dimensional spinor:

$$\left[\frac{\hat{\mathbf{p}}^2}{2m} + \mu_B \hat{\boldsymbol{\sigma}} \cdot \mathbf{B}_{xc} + \hat{V}_{eff} \right] |\phi_i\rangle = E |\phi_i\rangle, \quad (14)$$

where the field \mathbf{B}_{xc} is the exchange-correlation magnetic field, and \hat{V} is the effective Kohn-Sham potential. One way to interpret \mathbf{B}_{xc} is as the field generated by the set of electrons in the solid that tends to align their spins, represented by the Pauli operator $\hat{\boldsymbol{\sigma}}$ [7].

As the Pauli operator and the magnetic field have three components each, and the Pauli matrices do not commute with each other, the calculations become very complex if all components are taken into account. In other words, it is not practical to perform DFT calculations with an arbitrary spin orientation. In this way, one solution to this problem is to use the intrinsic spin orientation of a FM or AFM material, and defining this orientation as the z-axis of the problem. This technique is called spin-polarized calculation in the z-direction [7] and is used in this work. Thus, the equation reduces to:

$$\left[-\frac{\hbar^2}{2m} \nabla^2 + \mu_B B_{xc} \hat{\sigma}_z + \hat{V}_{eff} \right] |\phi_i\rangle = E |\phi_i\rangle. \quad (15)$$

As the Pauli matrix $\hat{\sigma}_z$ is diagonal, the eigenstates are given by:

$$|\phi_{i\uparrow}\rangle = \begin{pmatrix} \phi_{i\uparrow}(\mathbf{r}) \\ 0 \end{pmatrix}, \quad |\phi_{i\downarrow}\rangle = \begin{pmatrix} 0 \\ \phi_{i\downarrow}(\mathbf{r}) \end{pmatrix}, \quad (16)$$

with $|\phi_{i\uparrow}\rangle$ representing the spin-up state, and $|\phi_{i\downarrow}\rangle$ representing the spin-down state. Thus, finally,

we can define the electronic densities for spin-up and spin-down:

$$\rho_{\uparrow}(\mathbf{r}) = \sum_i |\phi_{i\uparrow}|^2, \quad \rho_{\downarrow}(\mathbf{r}) = \sum_i |\phi_{i\downarrow}|^2. \quad (17)$$

From all these definitions, we have the basis for understanding total and absolute magnetization's. Magnetization is defined as the magnetic moment per unit volume [8], and can be described by the two following quantities:

$$M_{tot} = \int d^3r (\rho_{\uparrow}(\mathbf{r}) - \rho_{\downarrow}(\mathbf{r})), \quad (18)$$

$$M_{abs} = \int d^3r |\rho_{\uparrow}(\mathbf{r}) - \rho_{\downarrow}(\mathbf{r})|, \quad (19)$$

where the integral is done in the whole unit cell. In a FM system, $M_{tot} = M_{abs} \neq 0$. On the other hand, in an antiferromagnetic system, $M_{abs} \neq M_{tot} = 0$. To handle a ferromagnetic system, the use of equation 15 in a spin-polarized calculation is sufficient. The energy values undergo a *shift* between the spin-up and spin-down states due to the diagonal elements of $\hat{\sigma}_z$ having values of ± 1 [7]. The DOS for a FM system is depicted in figure 4.

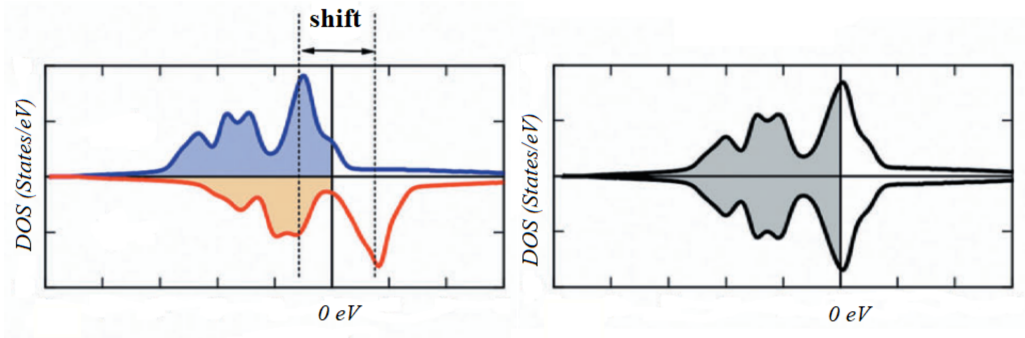


FIG. 4: The left figure represents the DOS obtained through spin-polarized FM calculation. The right figure a DOS obtained through non-spin-polarized calculation [7].

As mentioned earlier, a correction has to be implemented for the description of the Fe d electrons in FeO. This is a standard procedure for the so called strongly correlated systems. This correction is also useful for describing the AFM model and its direct implications, such as the magnetic exchange interaction between fermions [18], and its relationship with the lattice parameter, for example.

2.4. The strong-correlation puzzle

One can describe simple systems, *i.e.* where the kinetic energy of the electrons is much greater than the Coulomb interaction between them, well enough with the mathematical framework presented so far. However when dealing with materials in the limiting case where the Coulomb interaction is comparable, or even greater, to the kinetic energy, the so called strongly correlated systems, one needs corrections [23]. This is because, in the DFT perspective, the interactions between electrons are approximated on the V_H and V_{XC} terms of equation 9, causing loss of information about those interactions.

Those materials, however, are not just miss-explained by DFT. Strongly correlated systems are, in general, a great mystery in modern physics: from Mott insulators to complex magnetic systems [10]. In fact, strongly correlated phenomena can be understood as an emergent effect from localized states physics. Despite this, the description of strongly correlated systems is advancing [24]. Methods like DFT+U and DFT+DMFT as explicit correction to V_{XC} methods, and even symmetry breaking methodologies [25], are showing excellent results when compared with experimental data. In the present work, we explored the field of Mott insulators, with FeO as a prototypical example. But why FeO?

Iron (II) oxide is a Mott insulator: it is predicted as a metal by mean field like approximations (like DFT) but is an insulator experimentally. This happens due to the localized Fe d electrons on the system that tends to be related with strong correlation effects on TMO's [13]. In this way, a correction on the Fe d electrons is convenient, and is achieved by the DFT+U method, which is discussed in the next section.

This correction has the objective of applying an explicit Coulomb interaction term on the V_{XC} potential of equation 9. This kind of approach is achieved by relying on toy models, or model Hamiltonians, in this case the Hubbard model [12].

2.5. When strongly correlated systems meet DFT

The correction studied in this work for strongly correlated systems due to localization is based on the Hubbard model, which is essentially an extension of the tight-binding approximation approximation with the presence of a coulomb repulsion interaction [12]. The model is for non-relativistic

fermions with spin [26], in this case, electrons, and it is summarized in the Hubbard Hamiltonian:

$$\hat{H} = -t \sum_{\langle i,j \rangle \sigma} \left(\hat{c}_{i\sigma}^\dagger \hat{c}_{j\sigma} + \hat{c}_{j\sigma}^\dagger \hat{c}_{i\sigma} \right) + U \sum_i \hat{n}_{i\uparrow} \hat{n}_{i\downarrow}. \quad (20)$$

Here, $\hat{c}_{i\sigma}^\dagger$ represents the creation operator, which creates a fermion with spin σ on the site i , $\hat{c}_{j\sigma}$ is the annihilation operator, which annihilates a fermion in site j with spin σ , $\hat{n}_{i\sigma} = \hat{c}_{i\sigma}^\dagger \hat{c}_{i\sigma}$ is the number operator and it counts the number of electrons on site i with spin σ . The Hamiltonian is divided into the terms of kinetic energy, the first term on the RHS, and a potential term proportional to the Hubbard potential (parameter), which is the second term on the RHS. The Hubbard U is a crucial parameter in the DFT+U description.

In equation 20, t accounts for the nearest neighbor hopping probability amplitude, and U is the coulomb repulsive interaction between electrons. There is a competition between these two terms, and one is interested on the $t \ll U$ limit for localized states and strongly correlated physics. As one can observe in figure 5, correlation and localization are connected in this model, which is interesting for us since we are dealing with FeO.

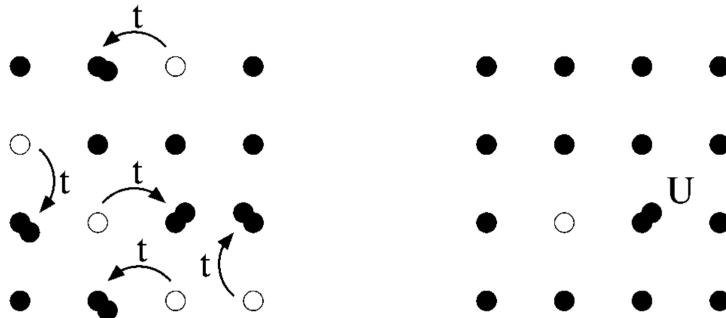


FIG. 5: Hubbard model illustration [12].

In this way, when dealing with the Hubbard Hamiltonian properly in the $t \ll U$ limit, *i.e.* applying mean field and perturbation theories, one can derive the Heisenberg Hamiltonian for a magnetic system:

$$\hat{H} = J \sum_{\langle i,j \rangle} \hat{\mathbf{S}}_i \cdot \hat{\mathbf{S}}_j. \quad (21)$$

In this expression, J representing the magnetic exchange term and the \mathbf{S} operators representing spin operators. In this case, $J = \frac{4t^2}{U} > 0$, which implies that the Hubbard model in the limit

of $t \ll U$ has an antiferromagnetic ground state, since the Heisenberg Hamiltonian predicts an antiferromagnetic ground state for $J > 0$ in the chosen notation.

Therefore, the idea of the DFT+U approach is to use a Hubbard-like Hamiltonian to describe the localized d electrons in FeO, and the standard KS Hamiltonian to describe the non-localized s and p electrons. Besides, this approach should be useful to calculate strongly correlated materials magnetic properties as well, as seen in the discussion above.

This approach is guaranteed by the potential above [27], which is added explicitly on the V_{eff} of equation 9:

$$\hat{V}_{XC}^U = U \sum_{im} \left(\frac{1}{2} - n_m^{i\sigma} \right) |m\rangle \langle m|, \quad (22)$$

where U is the Hubbard parameter. The $n_m^{i\sigma}$ term is the occupation matrix eigenvalue on the site i , localized state ($l > 1$) $|m\rangle$ and spin state σ . This potential acts only on localized states $|m\rangle \langle m| = \hat{P}_m$. A diagram of its action in the DFT+U context is shown below.

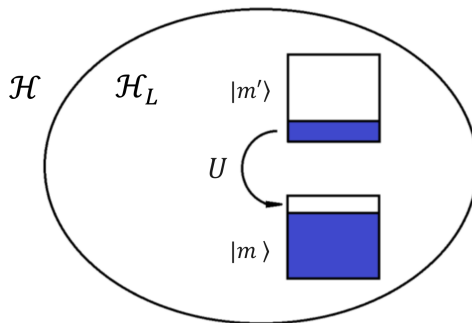


FIG. 6: Diagram of the DFT+U action.

Here, \mathcal{H} is the total Hilbert space of the system (spanned by the eigenstates of the KS Hamiltonian), \mathcal{H}_L is the localized Hilbert space (where the d states live), $|m\rangle$ and $|m'\rangle$ are localized states and U is the Hubbard parameter. Electron occupation on each state, which are the boxes, is represented by the blue filling. Since DFT is an energy minimization problem, minimizing the energy eigenvalues of \hat{V}_{XC}^U is obtained via transporting electrons from less-than-half occupied states ($|m'\rangle$ in the figure) to more-than-half occupied states ($|m\rangle$), always keeping the number of particles constant. This is easily concluded by analyzing the functional form of the \hat{V}_{XC} potential. This tends to split the levels, opening a gap mediated by the strength of the interaction U , completing the DFT+U description of materials.

3. COMPUTATIONAL METHODS

From a practical point of view, the software Quantum ESPRESSO (QE) [28–30] was used, which was already installed on the titanium cluster, the main machine of the UFABC CCM. QE is software designed to solve the Kohn-Sham equations iteratively, following the flowchart in Figure 3.

The software offers various types of available codes, and the most used in this work is pwscf (Plane Wave Self-Consistent Field). This code uses a plane wave expansion for the function $u_{n\mathbf{k}}(\mathbf{r})$, which takes the following form:

$$u_{n\mathbf{k}}(\mathbf{r}) = \sum_{\mathbf{G}} C_{\mathbf{G}} e^{i\mathbf{G}\cdot\mathbf{r}}, \quad (23)$$

where \mathbf{G} represents the allowed vectors in the first Brillouin zone [8]. By substituting Equation 23 into the Bloch function (Equation A2), one has:

$$\psi_{n\mathbf{k}}(\mathbf{r}) = \sum_{\mathbf{G}} C_{\mathbf{k}+\mathbf{G}} e^{i(\mathbf{k}+\mathbf{G})\cdot\mathbf{r}}. \quad (24)$$

The expansion is exact if the number of terms is infinite, which is computationally impractical. Therefore, there is a truncation of the series in the wave vector to a certain *cutoff* point \mathbf{G} . However, this point is translated into a cutoff energy, since equation 24 is an eigenfunction of the kinetic energy operator projected onto the position space, with eigenvalue $\epsilon = \frac{\hbar}{2m} |\mathbf{k} + \mathbf{G}|^2$. Thus, imposing a limit on ϵ implies a limit on \mathbf{G} , thereby truncating the series in Equations 23 and 24 [5].

The cutoff energy manifests itself in two forms: the wavefunction cutoff energy (*ecutwfc*), extracted from concepts present in Equation 24, and the electronic density cutoff energy (*ecutrho*). Therefore, the cutoff energies and the number of k -points, the mesh in reciprocal space with the aim of discretizing the domain to allow numerical integration, are the main parameters for computational optimization to be adjusted in the models.

The pwscf code offers various types of useful calculations for the objectives of this work:

- i.* *Scf* - a self-consistent calculation that uses the algorithm in Figure 3 to obtain the KS orbitals and energy eigenvalues of the system, using the Born-Oppenheimer approximation;
- ii.* *Nscf* - a non-self-consistent calculation. Knowing the KS orbitals from the *scf* step, this calculation uses Equation 10 to obtain $\epsilon_n(\mathbf{k})$. A commonly used technique is to increase the k -point grid in the *nscf* calculation to obtain a smoother dispersion relation.

iii. Vc-relax - an equivalent calculation to *scf*, but with ions being moved in the directions of the total forces, given by the equation below,

$$\mathbf{F}_I = f(\rho(\mathbf{r}), \mathbf{r}, \mathbf{R}_I),$$

to minimize the system's energy and optimize the structure [7]. The *vc* stands for *variable-cell*, meaning that the lattice vectors of the unit cell vary in this calculation.

It is notable from the above equation that the force on each nuclei \mathbf{I} on the system depends on the electron density. In other words, the nuclei movement depends on the KS orbitals for the electrons of the system, *i.e.* the solutions of the electronic system described by the KS equations.

iv. Relax - equivalent to *vc-relax*, but with fixed lattice vectors.

In addition to `pwscf`, the code `bands.x` is useful for the objectives of this work, as it allows us to obtain the band structure of the material and the density of states.

To solve the Kohn-Sham equations, it is necessary to have a starting point regarding the knowledge of the positions of the atoms involved in the problem. For this purpose, the crystalline structure of the system was created. FeO is a material with a face-centered cubic (FCC) structure, as shown in figure 7a. However, for the present project, the structure was constructed based on the ABC stacking of Fe and O atoms in the (111) plane, since the spins of the Fe atoms are oriented along the [111] vector, as indicated in figure 7b [31]. Twelve atom layers in total were used on the supercell in the z direction. On x and y directions, only one atom was used.

This approach was chosen so that spin-polarized calculations in the z -direction could be used through equation 15, simplifying the problem. Additionally, there was an interest in investigating the (111) surface of this material, contributing to the construction of the stacked structure in the [111] direction.

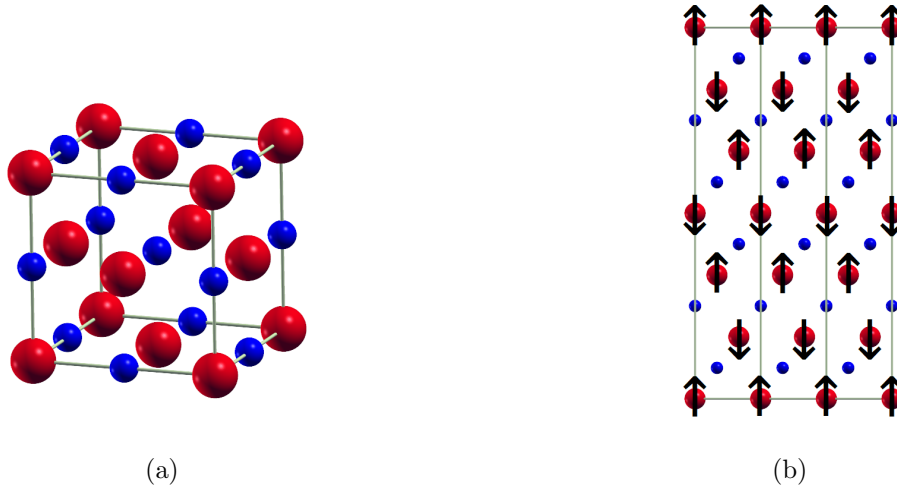


FIG. 7: (a) The face-centered cubic (FCC) bulk structure of FeO consists of Fe atoms represented in red, while O atoms are represented in blue. (b) Atoms stacked in the direction (111). Upward arrows represent spin-up states, and downward arrows represent spin-down states.

For the surface model, the slab technique was used [5], as shown in figure 8. Starting from the bulk model, a vacuum of sufficient size was opened so that, under periodic boundary conditions, the layers of atoms do not interact with each other.

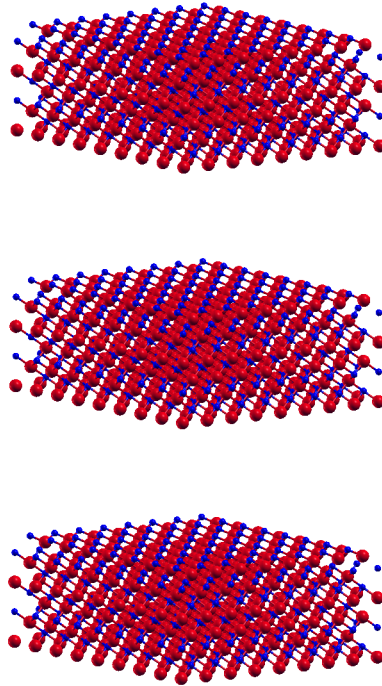


FIG. 8: An illustration of the slab model, the technique used in the present work to recreate surface states.

To conclude the methodology session, the main numerical parameters used in the models are shown below:

k-points - A Monkhorst-Pack mesh $5 \times 5 \times 5$ was used for the bulk. For the surface it was used a $5 \times 5 \times 1$ mesh.

ecutrho - A cutoff energy of 650 Ry was used for the charge density.

ecutwfc - A cutoff energy of 65 Ry was used for the wavefunctions.

σ - A $\sigma = 0.001 Ry$ was used with the Marzari-Vanderbilt distribution function [32].

It is important to mention that all parameters were chosen in order to optimize the model. Thus, all numerical values were obtained with convergence tests on the total energy of the system. The E_{XC} used is the GGA-PBE and the pseudopotential is the PAW [22].

4. OBJECTIVES

The objective of this work is to model the electronic and magnetic properties of FeO, a prototypical strongly correlated system, through DFT+U or GGA+U. The aim is to calculate bulk properties and leverage the vast availability of results in the literature to validate the theoretical model. Subsequently, the focus is shifted to investigate the electronic and magnetic properties of the (111) surface of this material. This poses a greater challenge due to the translational symmetry breaking induced by the surface. Additionally, the present work aims to introduce the student to the field of strongly correlated systems, which will be the main topic of his Ph.D. research.

5. RESULTS AND DISCUSSIONS

The results obtained from the calculations are divided into several sections. Firstly, the implemented Hubbard model in Quantum ESPRESSO was validated based on the expected results from the literature. This step was crucial to comprehend how the model behaves and to specify the occupations in the d orbitals [27].

After that, the results are divided into two parts: **1)** electronic, structural, and magnetic properties of the bulk; and **2)** electronic, structural, and magnetic properties of the (111) surface

terminated with oxygen. These latter calculations were performed using equation 12 and equation 15, which were already implemented in Quantum ESPRESSO itself.

It is worth noting that part of the results were obtained using non-polarized spin calculations. The context will make it clear when non-polarized or polarized spin calculations are being performed.

5.1. DFT+U validation

Qualitatively, the DFT+U (or GGA+U since we used the PBE functional) method, without altering the d states occupations, could lead to similar results obtained with DFT itself [27]. In this way, a good understanding of the occupation matrix eigenvectors and eigenvalues is extremely important. There are *five* eigenvectors, corresponding to each degenerate d state of the localized band, and *five* eigenvalues, representing each d state occupation.

By Crystal Field Theory (CFT), the continuous rotational symmetry breaking, by the octahedral FeO geometry, splits the five-fold degenerate d states into two sets with different energies [19]. One of these sets is triply degenerate (t_{2g}) and the other is doubly degenerate (e_g). In order to describe the FeO system as a Mott insulator, one should totally occupy the A_{1g} level, or the only level which have different occupation eigenvalue in the set of t_{2g} states [27].

All this discussion is, of course, meaningless without considering the DFT+U approach. In this way, The value of the Hubbard parameter U used in the present work was obtained through the *hp.x* code using Density Functional Perturbation Theory (DFPT) methods [27]. The obtained value was $U = 5.4 \text{ eV}$, which is in agreement with literature data, as shown in Table I:

Works	U value (eV)
Present project	5.4
Meng [13]	4
Zhang [33]	5
Zaanen [34]	5.1
Rodl [35]	≈ 5

TABLE I: Values of the Hubbard potential determined in the present work and in the literature.

Thus, on calculations involving the GGA+U method, the value of $U = 5.4 \text{ eV}$ is used. The combination of occupying the A_{1g} state and using $U = 5.4 \text{ eV}$ describes FeO properties properly, as one can see in the next sections.

5.2. Results and discussions for the bulk FeO

The bulk of FeO-B1 is experimentally antiferromagnetic at ambient pressure and temperature [14]. Therefore, predicting the ground state under these conditions was crucial for validating the model. A *scf* calculation using the GGA+U method was performed, varying the lattice parameter and, consequently, the volume of the unit cell for three magnetic configurations: antiferromagnetic (AFM), ferromagnetic (FM), and non-magnetic. The results are shown in figure 9.

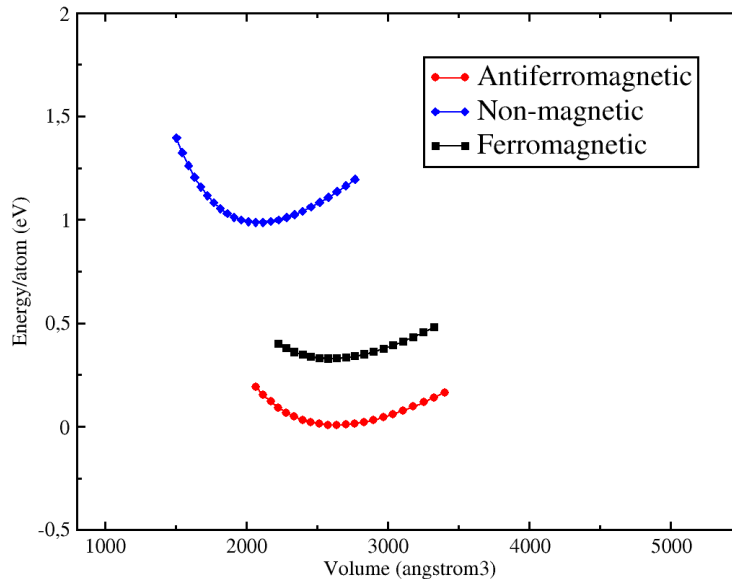


FIG. 9: Total energy vs. volume of the unit cell.

The zero energy was redefined for the AFM state. Consequently, the energy difference δE between the AFM and FM states is approximately $0.025 Ry$. Comparing this δE with $k_B T$ at room temperature, the results are shown in Table II:

$k_B T (meV)$	$\delta E (meV)$
25.7	340.1

TABLE II: Comparison between the energy scaling factor and the difference between the AFM and FM states.

It is evident that δE between the AFM and FM states is much greater than $k_B T$. Hence, the energy available at room temperature is not sufficient to induce a magnetic phase transition, and the ground state of the bulk remains AFM at ambient temperature. This result is expected from experimental results and for the limit $t \ll U$ for the Hubbard model, as discussed earlier.

After analyzing the spin-polarized calculations on the AFM configuration, it was observed that the total and absolute magnetization values converged to the following values:

$$M_{tot} = 0 \mu_B/cell,$$

$$M_{abs} = 21.17 \mu_B/cell,$$

which agrees with the literature and with the AFM state predicted in figure 9. The individual magnetization at each Fe atom was consistent with the literature data [13, 14], where the former reported experimental magnetization per Fe atom of $3.32 \mu_B$ to $4.2 \mu_B$, and the latter obtained first-principles calculation results of approximately $3.5 \mu_B$ for the experimental volume of the FCC unit cell. Residual magnetization in the Oxygen atoms was observed, which is expected. The range obtained in the calculations is between $3.23 \mu_B$ and $3.67 \mu_B$.

The DOS of the bulk FeO-B1 AFM structure is shown in figure 10. The density of states is, of course, a great tool to evaluate electronic properties, but also to obtain some magnetic features, as well. As one can observe, the DOS is symmetric for up and down-spin, indicating an AFM configuration, as expected.

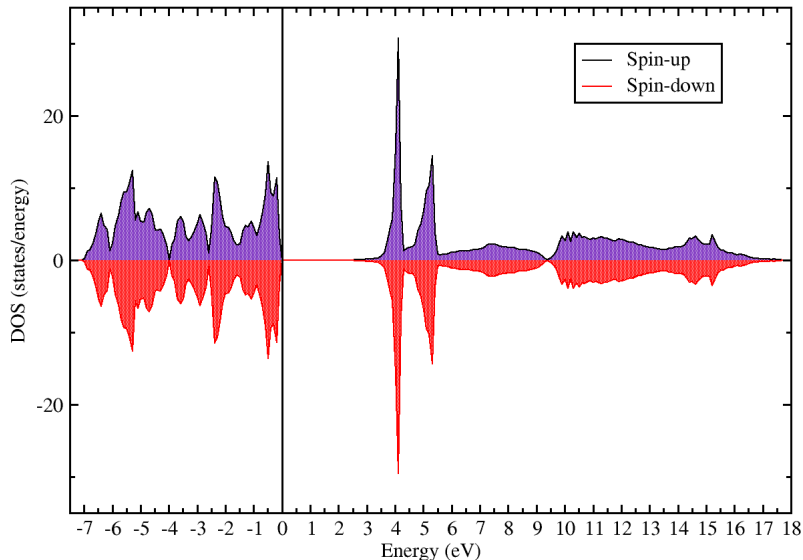


FIG. 10: DOS of FeO obtained through the spin polarized GGA+U.

This result was obtained with the GGA+U method with $U = 5.4 eV$. As mentioned earlier, FeO is a Mott insulator in its ground state. However, when performing a *vc-relax* calculation with non-polarized spin, followed by *dos.x* calculation for FeO using the GGA method, it exhibits metallic behavior, as indicated in figure 11. The zero energy corresponds to the Fermi level.

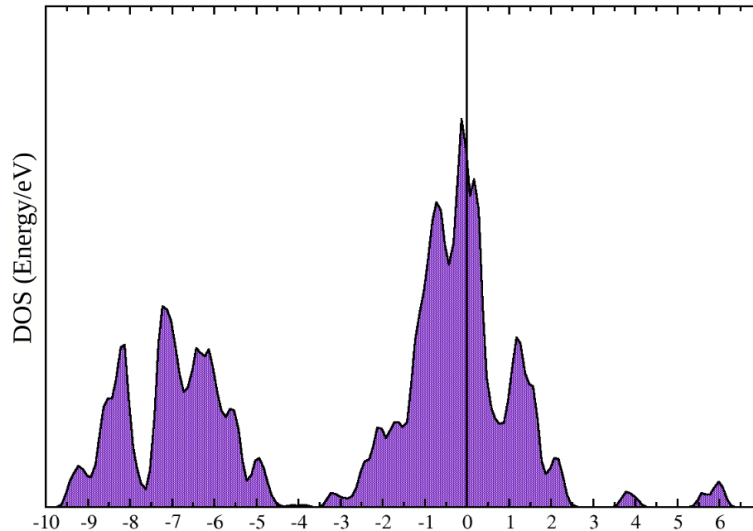


FIG. 11: DOS of FeO obtained through the non-polarized spin GGA calculation.

This is the main result which indicates the importance of using the GGA+U methodology to deal with a Mott insulator [13]. The obtained band-gap from the GGA+U calculation is approximately 2.4 eV, which also agrees with the results from the literature [13, 35, 36].

With respect to the FeO structural properties, experiments suggest that the cubic lattice parameter takes values of $a = 4.33$ Å. In the GGA+U description for electrons in the d state, the lattice parameter obtained was $a_{GGA+U} = 4.43$ Å, in contrast with $a_{GGA} = 4.27$ Å, obtained without the U correction. Structural, electronic and magnetic properties are summarized in table III.

Method or Source	a (Å)	MM (μ_B)	Band gap (eV)
GGA	4.27	-	<i>metallic</i>
GGA+U	4.43	3.23 - 3.67	2.4
Ab. initio. lit	4.34 [13]	3.5 [37]	2.4 [35, 36]
Experimental	4.33 [13]	3.32 - 4.2	2.4 [13]

TABLE III: A comparison between the GGA and GGA+U methods calculated in this work, and data available in the literature.

5.3. Results and discussions for the (111) surface

The next step was to apply the developed and validated model of FeO bulk to the (111) surface using the oxygen-terminated slab technique. The same energy analysis as shown in figure 9 was

performed for the surface, but without varying the lattice parameter.

The choice of the AFM configuration for the surface is justified by the experimental and theoretical results in the current study for the bulk, as well as being supported by works such as that of Bernal-Villamil and Gallego [38], which predicts the (111) surface to exhibit antiferromagnetic behavior. The FM surface model was based on the works of Koike and Furukawa; Li, Yao, Liu, and Gao; Mori, Yamazaki, Hiraki, Matsuyama, and again Koike [39–41]. The energies of the magnetic configurations are shown in figure 12:

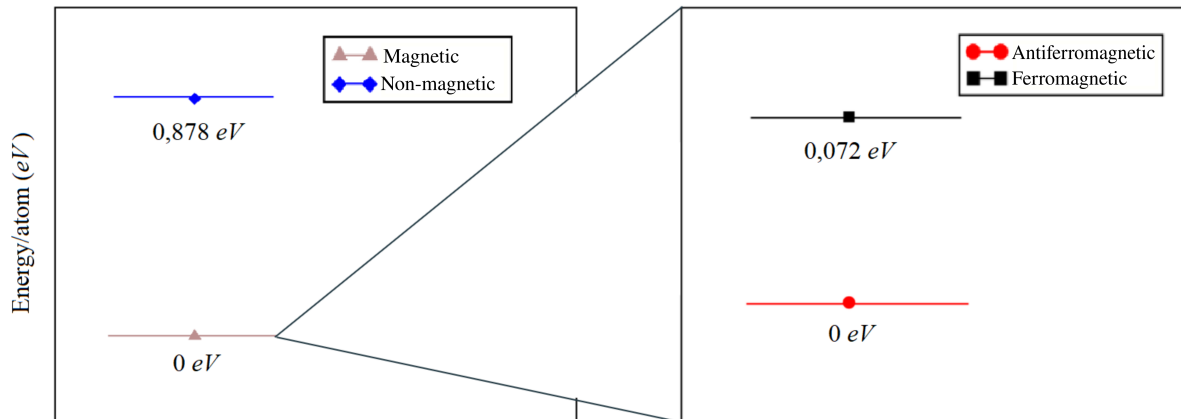


FIG. 12: Energies of the FM, AFM, and non-magnetic states.

It can be observed that the initially degenerate magnetic states differentiate in more accurate calculations. The energy difference between the ferromagnetic and antiferromagnetic surfaces (δE_{FM-AFM}) is approximately 0.072 eV. As a result, according to table II, $\delta E_{FM-AFM} > k_B T$, and the ground state, even at room temperature, remains antiferromagnetic according to the model proposed in this study. However, since both δE_{FM-AFM} and $k_B T$ exhibited the same order of magnitude, numerical errors or flaws in the model itself might be affecting the results. As a result, it was considered that both states are thermodynamically probable at room temperature. In this way, the DOS of both FM and AFM states for the (111) surface of FeO were evaluated.

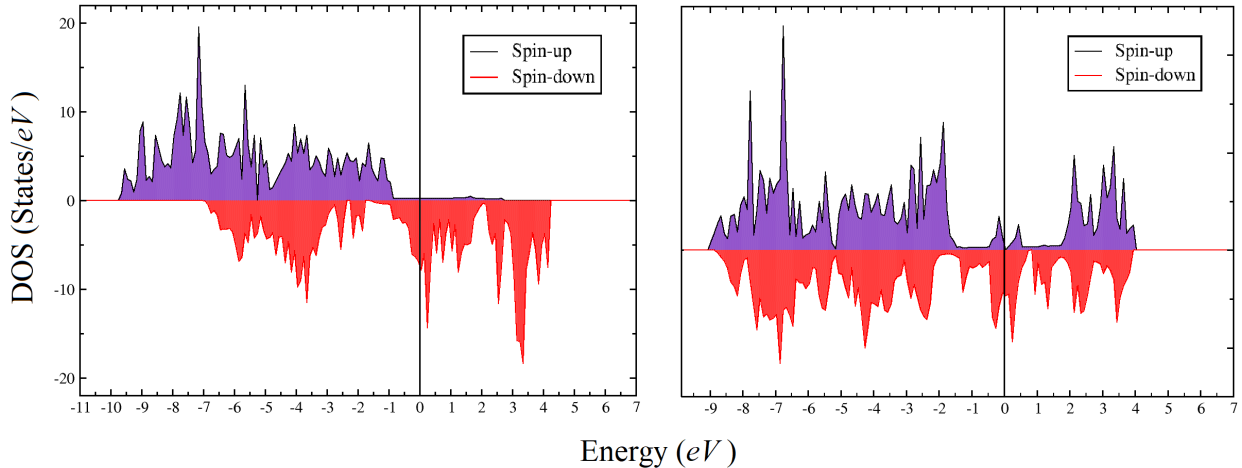


FIG. 13: FM surface DOS on the left. AFM surface DOS on the right

The ferromagnetic solution is noticeable in accordance with the theoretical description through equation 15 and figure 4 in section 2.2.3. Additionally, it is evident that the FM state for the (111) surface of FeO is metallic, as the Fermi level resides inside the valence band of the spin-down states. This result was also obtained by Li, Yao, Liu, and Gao [40]. The surface with the AFM configuration also exhibits metallic behavior, which supports the conclusion of our model that the (111) surface of FeO is indeed conductive in its ground state, intriguingly opposite to the bulk ground state for FeO-B1.

The analysis of the magnetic properties of the FM state begins with its own definition. The calculations for this configuration converged to a FM structure with Fe atoms magnetic moments varying from $3.26 \mu_B$ to $3.85 \mu_B$. The Fe atoms closer to the surface have the biggest magnetic moments. One also observes the proximity of the absolute values of magnetization per atom to those presented in the bulk. The model predicted the total and absolute magnetizations as shown below:

$$M_{tot} = 24.56 \mu_B/cell,$$

$$M_{abs} = 24.67 \mu_B/cell,$$

The increase in the magnitude of M_{abs} compared to the bulk can be associated with the breaking of translational symmetry at the surface, as the high magnetization, when compared to bulk values, occurred in atoms closer to the surface.

In the AFM configuration, the calculations converged to an AFM structure with Fe atoms magnetic moments varying in absolute value from $3.32 \mu_B$ to $3.64 \mu_B$. The amplification effect of

the magnetic moment, possibly due to the low symmetry of the surface, is also present in the AFM state, albeit in a more subtle manner. The values of total and absolute magnetization are:

$$M_{tot} = -0.02 \mu_B/cell,$$

$$M_{abs} = 23.60 \mu_B/cell,$$

The value of M_{Total} is very close to zero, and this difference could arise from numerical approximations. For practical purposes, therefore, the total magnetization confirms the antiferromagnetic state of the AF surface. It's interesting to note that even though the DOS isn't entirely symmetric, as shown in Figure 13, the AFM configuration still has $M_{Total} \approx 0 \mu_B/cell$, which indicates that the total number of states for spin-up and spin-down are equal below the Fermi energy.

Finally, with the translational symmetry breaking, the coordination number of the most surface atoms is reduced, and consequently, a relaxation process occurs in the outermost layers of the material [5]. This process was simulated in the current study, and the illustration of this phenomenon is elucidated in Figure 14:

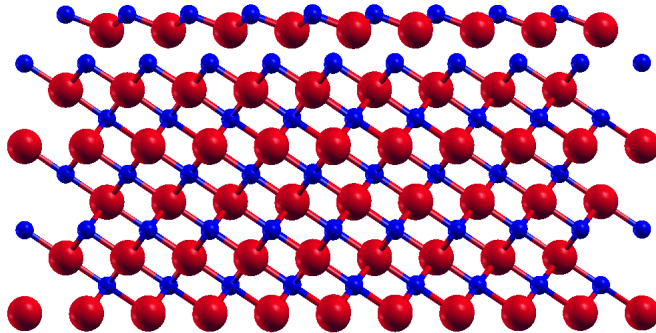


FIG. 14: Relaxation of the top 4 layers of the (111) surface of FeO-B1.

It is noticeable in the figure that the first two layers, or the first bilayer, are the ones most affected by the relaxation process. Following the notation of David Sholl [5], which is widely used in the literature, the new distances were evaluated for the 1 – 2 and 2 – 3 layers in terms of relative variation compared to the bulk lattice parameter, in percentage. This was done for the FM, AFM, and non-magnetic models:

2 relaxed bilayers	$\delta_{12}(\%)$	$\delta_{23}(\%)$
No mag	-36.00	7.96
AFM	-42.79	18.72
FM	-42.21	18.76

TABLE IV: Relative variations (compared with the bulk lattice parameter) of layers 1-2 and 2-3 for the different magnetic states.

There is a greater variation between the layers when magnetism is taken into account. This can occur due to the interaction of the magnetic field resulting from spins with the charges of the nuclei and the electronic density of the crystal.

6. CONCLUSIONS

In this work, we calculated the electronic and magnetic properties of FeO via DFT+U. The results for the bulk are in good agreement with the literature. The Hubbard potential obtained via first principles, $U = 5.4 \text{ eV}$, is close to values found in distinct papers. The predicted ground state is AFM, just like in the literature. The calculated lattice parameter is slightly overestimated compared to the experimental value, but the error is expected by the usage of the PBE functional. The electronic and magnetic properties of the bulk were accurately reproduced by the model. The bulk results were of great utility for the validation of the theoretical model.

When extrapolating the model to the (111) surface of FeO, some interesting results emerged. The model predicted an AFM state as the ground state at absolute zero. At room temperature, the energy difference between the AF and ferromagnetic (FM) states is on the order of $k_B T$ at room temperature. Therefore, the remaining properties were calculated for both magnetic configurations. The first two layers of the surface experienced greater displacement when the system's magnetism is taken into account. Furthermore, the model predicted that the surface of both configurations are metallic.

Appendix A: Bloch theorem derivation

Considering the Hamiltonian of a 1D crystal

$$\hat{H} = \frac{\hat{p}^2}{2m} + V(\hat{x}),$$

where $V(\hat{x}) = V(\hat{x} + a)$ with a being the period of the lattice, as shown in figure 1. One can define the translation operator \hat{T}_n , which acts on a state as follows:

$$\hat{T}_n \psi(x) = \psi(x + na). \quad (\text{A1})$$

Here, a is again the lattice parameter and n is an integer. It is clear that, since the potential is periodic and the momentum is the generator of the translation operator, $[\hat{H}, \hat{T}_n] = 0$. This configures a symmetry in the Hamiltonian, which means that \hat{T}_n and \hat{H} share the same eigenstates. We can calculate them:

$$\hat{T}_n \psi(x) = \lambda_n \psi(x).$$

The operator must be additive:

$$\hat{T}_{n_1} \hat{T}_{n_2} \psi(x) = \hat{T}_{n_1+n_2} \psi(x),$$

which implies in $\lambda_{n_1} \lambda_{n_2} = \lambda_{n_1+n_2}$, and must respect the normalization condition, where V is the total volume of the 1st Brillouin zone:

$$1 = \int_V |\psi(x)|^2 dx = \int_V |\hat{T}_n \psi(x)|^2 dx = |\lambda_n|^2 \int_V |\psi(x)|^2 dx = |\lambda_n|^2,$$

which gives \hat{T}_n 's eigenvalues the following form:

$$\lambda_n = e^{ikna}.$$

One can reinsert the eigenvalue in the definition of the translation operator, equation A1:

$$\hat{T}_n \psi(x) = \psi(x + na) = e^{ikna} \psi(x),$$

and this condition is always true for a Bloch wavefunction:

$$\psi_k(x) = e^{ikx} u_k(x), \quad (\text{A2})$$

where $u_k(x) = u_k(x + na)$. The extrapolation to a 3D system is straightforward, leading to:

$$\psi_{n\mathbf{k}}(\mathbf{r}) = e^{i\mathbf{k}\cdot\mathbf{r}} u_{n\mathbf{k}}(\mathbf{r}) \quad \blacksquare$$

Where the subindex n denotes the energy eigenstate.

Appendix B: Schrödinger equation in periodic potentials

Following from equation 5, one can replace the Bloch wavefunction, $\psi_{n\mathbf{k}}(\mathbf{r}) = u_{n\mathbf{k}}(\mathbf{r})e^{i\mathbf{k}\cdot\mathbf{r}}$ into the Schrödinger equation. Using that $\nabla e^{i\mathbf{k}\cdot\mathbf{r}} = i\mathbf{k}e^{i\mathbf{k}\cdot\mathbf{r}}$:

$$\begin{aligned} & \left[-\frac{\hbar^2}{2m}\nabla^2 + \hat{V} \right] \left(u_{n\mathbf{k}}(\mathbf{r})e^{i\mathbf{k}\cdot\mathbf{r}} \right) = E \left(u_{n\mathbf{k}}(\mathbf{r})e^{i\mathbf{k}\cdot\mathbf{r}} \right) \Rightarrow \\ & \Rightarrow -\frac{\hbar^2}{2m}\nabla^2 \left(u_{n\mathbf{k}}(\mathbf{r})e^{i\mathbf{k}\cdot\mathbf{r}} \right) + \hat{V} \left(u_{n\mathbf{k}}(\mathbf{r})e^{i\mathbf{k}\cdot\mathbf{r}} \right) = E \left(u_{n\mathbf{k}}(\mathbf{r})e^{i\mathbf{k}\cdot\mathbf{r}} \right) \Rightarrow \\ & \Rightarrow -\frac{\hbar^2}{2m}\nabla \cdot \left[i\mathbf{k}e^{i\mathbf{k}\cdot\mathbf{r}} u_{n\mathbf{k}}(\mathbf{r}) + e^{i\mathbf{k}\cdot\mathbf{r}} \nabla u_{n\mathbf{k}}(\mathbf{r}) \right] + \hat{V} \left(u_{n\mathbf{k}}(\mathbf{r})e^{i\mathbf{k}\cdot\mathbf{r}} \right) = E \left(u_{n\mathbf{k}}(\mathbf{r})e^{i\mathbf{k}\cdot\mathbf{r}} \right), \end{aligned}$$

which results in:

$$\begin{aligned} & -\frac{\hbar^2}{2m} \left[i\mathbf{k} \cdot \left(i\mathbf{k}e^{i\mathbf{k}\cdot\mathbf{r}} u_{n\mathbf{k}}(\mathbf{r}) + e^{i\mathbf{k}\cdot\mathbf{r}} \nabla u_{n\mathbf{k}}(\mathbf{r}) \right) + i\mathbf{k} \cdot e^{i\mathbf{k}\cdot\mathbf{r}} \nabla u_{n\mathbf{k}}(\mathbf{r}) + e^{i\mathbf{k}\cdot\mathbf{r}} \nabla^2 u_{n\mathbf{k}}(\mathbf{r}) \right] + \\ & + \hat{V} \left(u_{n\mathbf{k}}(\mathbf{r})e^{i\mathbf{k}\cdot\mathbf{r}} \right) = E \left(u_{n\mathbf{k}}(\mathbf{r})e^{i\mathbf{k}\cdot\mathbf{r}} \right). \end{aligned}$$

Distributing the factor $i\mathbf{k}$ to the first term inside the parentheses:

$$\begin{aligned} & -\frac{\hbar^2}{2m} \left(-k^2 u_{n\mathbf{k}}(\mathbf{r})e^{i\mathbf{k}\cdot\mathbf{r}} + i\mathbf{k} \cdot \nabla u_{n\mathbf{k}}(\mathbf{r})e^{i\mathbf{k}\cdot\mathbf{r}} + i\mathbf{k} \cdot \nabla u_{n\mathbf{k}}(\mathbf{r})e^{i\mathbf{k}\cdot\mathbf{r}} + \nabla^2 u_{n\mathbf{k}}(\mathbf{r})e^{i\mathbf{k}\cdot\mathbf{r}} \right) + \\ & + \hat{V} \left(u_{n\mathbf{k}}(\mathbf{r})e^{i\mathbf{k}\cdot\mathbf{r}} \right) = E \left(u_{n\mathbf{k}}(\mathbf{r})e^{i\mathbf{k}\cdot\mathbf{r}} \right). \end{aligned}$$

One can factor the term $e^{i\mathbf{k}\cdot\mathbf{r}}$ out from both sides of the equation:

$$\begin{aligned} & -\frac{\hbar^2}{2m} \left(-k^2 u_{n\mathbf{k}}(\mathbf{r}) + 2i\mathbf{k} \cdot \nabla u_{n\mathbf{k}}(\mathbf{r}) + \nabla^2 u_{n\mathbf{k}}(\mathbf{r}) \right) + \hat{V} u_{n\mathbf{k}}(\mathbf{r}) = E u_{n\mathbf{k}}(\mathbf{r}) \Rightarrow \\ & \Rightarrow \frac{\hbar^2}{2m} \left(k^2 - 2i\mathbf{k} \cdot \nabla - \nabla^2 \right) u_{n\mathbf{k}}(\mathbf{r}) + \hat{V} u_{n\mathbf{k}}(\mathbf{r}) = E u_{n\mathbf{k}}(\mathbf{r}) \end{aligned}$$

Simplifying the first term in parentheses, using $(k^2 - 2i\mathbf{k} \cdot \nabla - \nabla^2) = (-i\nabla + \mathbf{k})^2$:

$$\begin{aligned} & \frac{\hbar^2}{2m} (-i\nabla + \mathbf{k})^2 u_{n\mathbf{k}}(\mathbf{r}) + \hat{V} u_{n\mathbf{k}}(\mathbf{r}) = E u_{n\mathbf{k}}(\mathbf{r}) \Rightarrow \\ & \Rightarrow \frac{1}{2m} (-i\hbar\nabla + \hbar\mathbf{k})^2 u_{n\mathbf{k}}(\mathbf{r}) + \hat{V} u_{n\mathbf{k}}(\mathbf{r}) = E u_{n\mathbf{k}}(\mathbf{r}) \Rightarrow \\ & \left[\frac{1}{2m} (-i\hbar\nabla + \hbar\mathbf{k})^2 + \hat{V} \right] u_{n\mathbf{k}}(\mathbf{r}) = E u_{n\mathbf{k}}(\mathbf{r}) \quad \blacksquare \end{aligned}$$

This is, finally, the Schrödinger equation in a periodic potential, due to Bloch's theorem [7, 8].

References

- [1] M. Thomson, *Modern Particle Physics*, Modern Particle Physics (Cambridge University Press, 2013).
- [2] O. I. Mal'yi, G. M. Dalpian, X.-G. Zhao, Z. Wang, and A. Zunger, *Materials Today* **32**, 35 (2020).
- [3] M. Vondráček, L. Cornils, J. Minár, J. Warmuth, M. Michiardi, C. Piamonteze, L. Barreto, J. A. Miwa, M. Bianchi, P. Hofmann, L. Zhou, A. Kamlapure, A. A. Khajetoorians, R. Wiesendanger, J.-L. Mi, B.-B. Iversen, S. Mankovsky, S. Borek, H. Ebert, M. Schüler, T. Wehling, J. Wiebe, and J. Honolka, *Physical Review B* **94** (2016), 10.1103/physrevb.94.161114.
- [4] P. Dirac, *Proceedings of the Royal Society of London. Series A, Containing Papers of a Mathematical and Physical Character* **123**, 714 (1929).
- [5] D. Sholl and J. Steckel, *Density Functional Theory: A Practical Introduction* (Wiley, 2011).
- [6] W. Tung, *Group Theory in Physics* (World Scientific, 1985).
- [7] F. Giustino, *Materials Modelling Using Density Functional Theory: Properties and Predictions* (Oxford University Press, 2014).
- [8] C. Kittel, *Introdução a física do estado sólido* (LTC, 2006).
- [9] P. Hohenberg and W. Kohn, *Phys. Rev.* **136**, B864 (1964).
- [10] J. Quintanilla and C. Hooley, *Physics World* **22**, 32 (2009).
- [11] R. Kuzian, *Nanomaterials* **13**, 238 (2023).
- [12] D. P. Arovas, E. Berg, S. A. Kivelson, and S. Raghu, *Annual Review of Condensed Matter Physics* **13**, 239 (2022).
- [13] Y. Meng, X.-W. Liu, C.-F. Huo, W.-P. Guo, D.-B. Cao, Q. Peng, A. Dearden, X. Gonze, Y. Yang, J. Wang, H. Jiao, Y. Li, and X.-D. Wen, *Journal of Chemical Theory and Computation* **12**, 5132 (2016).
- [14] P. Zhang, R. E. Cohen, and K. Haule, *Journal of Physics: Conference Series* **827**, 012006 (2017).
- [15] R. Shankar, *Principles of quantum mechanics* (Plenum, New York, NY, 1980).
- [16] J. J. Sakurai and J. Napolitano, *Modern quantum mechanics; 2nd ed.* (Addison-Wesley, San Francisco, CA, 2011).
- [17] R. Martin, *Electronic Structure: Basic Theory and Practical Methods* (Cambridge University Press, 2004).
- [18] D. Griffiths, *Introduction to Quantum Mechanics* (Cambridge University Press, 2017).
- [19] M. Dresselhaus, G. Dresselhaus, and A. Jorio, *Group Theory: Application to the Physics of Condensed Matter* (Springer Berlin Heidelberg, 2007).
- [20] R. Eisberg and R. Resnick, *Quantum Physics of Atoms, Molecules, Solids, Nuclei, and Particles* (Elsevier, 1979).
- [21] K. Capelle, "A bird's-eye view of density-functional theory," (2002).

- [22] J. P. Perdew, K. Burke, and M. Ernzerhof, *Physical Review Letters* **77**, 3865 (1996).
- [23] S. Paschen and Q. Si, *Nature Reviews Physics* **3**, 9 (2020).
- [24] S. Lee, W. Park, H. Nakata, M. Filatov, and C. H. Choi, *Bulletin of the Korean Chemical Society* **43**, 17 (2021).
- [25] A. Zunger, *Nature Computational Science* **2**, 529 (2022).
- [26] R. Shankar, *Quantum Field Theory and Condensed Matter: An Introduction* (Cambridge University Press, 2017).
- [27] M. Cococcioni and S. de Gironcoli, *Physical Review B* **71** (2005), 10.1103/physrevb.71.035105.
- [28] P. Giannozzi *et al.*, *J. Phys.:Condens. Matter* **21** (2009).
- [29] P. Giannozzi *et al.*, *J. Phys.:Condens. Matter* **29** (2017).
- [30] P. Giannozzi *et al.*, *J. Phys.:Condens. Matter* **152** (2020).
- [31] A. Schrön and F. Bechstedt, *Physical Review B* **92** (2015), 10.1103/physrevb.92.165112.
- [32] N. Marzari and D. Vanderbilt, *Physical Review B* **56**, 12847 (1997).
- [33] W.-B. Zhang, Y.-H. Deng, Y.-L. Hu, K.-L. Han, and B.-Y. Tang, *Solid State Communications* **142**, 6 (2007).
- [34] J. Zaanen and G. Sawatzky, *Journal of Solid State Chemistry* **88**, 8 (1990).
- [35] C. Rödl, F. Fuchs, J. Furthmüller, and F. Bechstedt, *Physical Review B* **79** (2009), 10.1103/physrevb.79.235114.
- [36] F. Tran and P. Blaha, *Physical Review Letters* **102** (2009), 10.1103/physrevlett.102.226401.
- [37] I. I. Mazin and V. I. Anisimov, (1996), 10.48550/ARXIV.COND-MAT/9610147.
- [38] I. Bernal-Villamil and S. Gallego, *Phys. Rev. B* **94**, 075431 (2016).
- [39] K. Koike and T. Furukawa, *Phys. Rev. Lett.* **77**, 3921 (1996).
- [40] Y. L. Li, K. L. Yao, Z. L. Liu, and G. Y. Gao, *Phys. Rev. B* **72**, 155446 (2005).
- [41] K. Mori, M. Yamazaki, T. Hiraki, H. Matsuyama, and K. Koike, *Phys. Rev. B* **72**, 014418 (2005).